Admixture of excited states and ground states of a Eu^{3+} ion in $Eu_3Fe_5O_{12}$ by means of magnetic circular dichroism

M. Mizumaki
Japan Synchrotron Radiation Research Institute, SPring-8, 1-1-1 Kouto, Mikazuki-cho, Sayo-gun, Hyogo 679-5198, Japan

T. Uozumi
Osaka Prefecture University, 1-1 Gakuen-cho, Sakai-shi, Osaka 599-8531, Japan

A. Agui
Synchrotron Radiation Research Center Japan Atomic Energy Research Institute, SPring-8, 1-1-1 Kouto, Mikazuki-cho, Sayou-gun, Hyogo 679-5148, Japan

N. Kawamura and M. Nakazawa
Japan Synchrotron Radiation Research Institute, SPring-8, 1-1-1 Kouto, Mikazuki-cho, Sayoh-gun, Hyogo 679-5198, Japan
(Received 22 January 2004; revised manuscript received 8 January 2005; published 22 April 2005)

The soft x-ray absorption spectroscopy (XAS) and magnetic circular dichroism (MCD) have been measured around the $M_{4,5}$ edges at $T=20$ and 300 K in order to investigate the electronic states of Eu^{3+} ions in $Eu_3Fe_5O_{12}$. We found a structure in both the XAS and MCD spectra, which was not observed at $T=20$ K, on the lower energy side of the M_5 edge at room temperature. By using atomic model calculations, the origin of the structure is assumed to be due to the thermal effect for the degree of admixture of the excited states ($J=1$, 2) and ground states ($J=0$) of Eu^{3+}. Developing the linear response model to investigate the magnetic moment obtained from the experimental spectra, we conclude that the thermal excited states of Eu^{3+} ions is the linear combination between $J=0$, 1, and 2 and the magnetic-field-excited state is the quantum-mechanically mixed state of the ground and excited states.

DOI: 10.1103/PhysRevB.71.134416 PACS number(s): 75.50.Gg, 78.70.Dm

I. INTRODUCTION

Europium iron garnet (=EuIG) has been studied for a long time by many researchers as a typical ferrimagnetic material.[1–5] From the point of view of the study of the electronic state of Eu^{3+} in EuIG, the effect of the mixing of the ground state and excited state at finite temperature has not been well understood. In the isolated Eu^{3+} ion, the electronic state is the ground state with $J=0$. The energy difference between the ground state with $J=0$ and the excited states with $J=1$, 2 is in the degree of 300 K. The ground state of Eu^{3+} ion, therefore, easily admixes $J=0$ with $J=1$, 2 by thermal excitation. In fact, the environment of Eu^{3+} is not simple since the Eu^{3+} ion is surrounded by Fe^{3+} ions in EuIG and affected by the internal field from the iron spins. The magnetic moment of Eu^{3+} ions is coupled with that of magnetic Fe^{3+} ions at the octahedral site antiferromagnetically and that of Fe^{3+} ions at the tetrahedral site ferromagnetically (See Fig. 1).[2] From these points of view, EuIG is a good candidate to investigate how the electronic states of Eu^{3+} ion are affected by the external field of temperature and magnetic field. The excited states of Eu^{3+} ion in EuIG were induced by thermal energy and the magnetic field. The thermal excited states are the linear combination between $J=0$, 1, and 2. On the other hand, by analyzing the results of magnetic measurements[4] and Mössbauer measurements,[5] the magnetic-field-excited states are quantum-mechanically mixed with $J=0$, 1, and 2. However the characteristic contribution from the thermal and

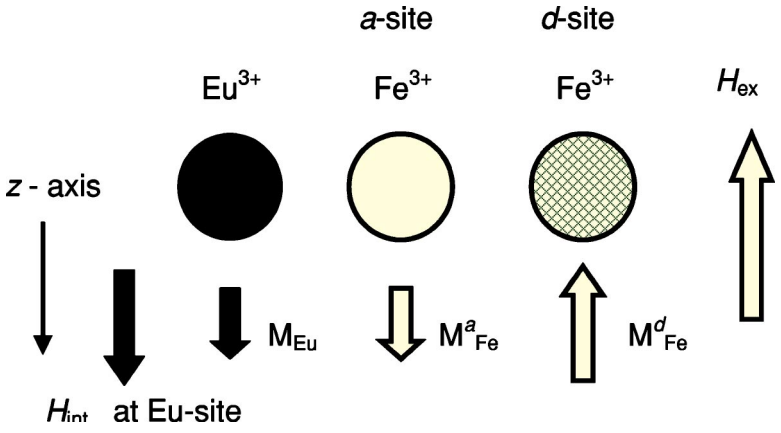

FIG. 1. Schematic representation of the magnetic-moment array in EuIG. The open, hatched, and closed circles represent a Fe^{3+} ion at the a site, a Fe^{3+} ion at the d site, and Eu^{3+} ions, respectively. M_{Eu} represents the magnetic moment of a Eu ion, and $M^{a(d)}{}_{Fe}$ represents the magnetic moment of an Fe ion at the $a(d)$ site. H_{ex} denotes the external field, while H_{int}, the internal field at the Eu sites. We define the z axis along with H_{int} in this study.

 ©2005 The American Physical Society

the magnetic excitation to excited states has never been studied separately. To investigate these contributions separately, the x-ray absorption spectroscopy (XAS) measurements for the thermal excitation and magnetic circular dichroism (MCD) measurements for the magnetic excitation can be used.

XAS measurements enable us to extract the electronic state of the specified element when the absorption edge was selected. Moreover, using MCD measurements, the magnetic properties with the specified element and orbital can be investigated. XAS around the Eu $M_{4,5}$ edges, which corresponds to transition from $3d$ to $4f$ orbital, can be used to directly measure the Eu $4f$ electronic states. Because the $4f$ electronic states of Eu bear its magnetism it is expected that the electronic state change due to thermal excitation will appear as the XAS spectral change. The MCD around the Eu $M_{4,5}$ edges should not be observed in the ground state of the Eu^{3+} ion because the ideal ground state of the Eu^{3+} ion has no magnetic moment. However, if Eu^{3+} ions have the excited states as a results of a magnetic field, the MCD effect would appear, and the magnetic properties of the Eu^{3+} ion in EuIG could be investigated. In addition, the orbital magnetic moments are estimated by applying the magneto-optical sum rule (the so-called L_z sum rule) to XAS and MCD spectra.[6,7] At $T=0$ K, the expected value of the J_z of the Eu^{3+} ion is zero and the total magnetic moment is equal to the orbital magnetic moment.

In this paper, we discuss the electronic state of Eu^{3+} ions in EuIG under the internal field and at finite temperature. The experimental method of XAS and MCD measurement is described in Sec. II A. In Sec II B, we describ the state of the experimental result, in which the excited states $J=1$, 2 are observed. In Sec. III, the method of full-multiplet calculation, including the internal magnetic field and a finite temperature, is given. In Sec. IV A, the XAS spectral change due to thermal excitation is discussed by using theoretical calculations. In Sec. IV B, we discuss the origin of the MCD effect at low temperature. In Sec. IV C, the total magnetic moment is estimated by using the L_z sum rule and the temperature dependence of the magnetic moment is explained by the linear response model. In Sec. IV D, the relationship between the magnetic moment and the internal field is investigated by the linear response model. The results and discussions are summarized in Sec. V.

II. EXPERIMENT

A. Experimental Method

The Eu $3d$ XAS of EuIG was measured using synchrotron radiation at soft x-ray beamline BL23SU of SPring-8, Japan. The light source (ID23) was an APPLE-2 type variably polarizing undulator. The phase shift of the magnet rows of the undulator provides a switching of the helicity of the circularly polarizing soft x ray. The MCD measurement system, which was synchronized with a monochromator controlling the helicity, has a good signal-to-noise ratio with high energy resolution.[9] The optical system of BL23SU is a varied space plane grating-type monochromator. The energy resolution was set at $E/\Delta E \geqslant 7000$ around the Eu $M_{4,5}$ edges for the present study.

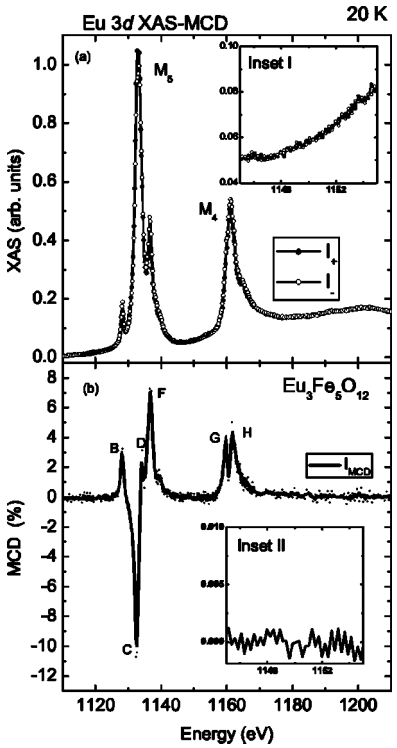

FIG. 2. (a) Experimental Eu $3d$ XAS of EuIG observed at 20 K. Solid (open) circles represent the XAS intensity $I_+(I_-)$ for the circularly polarized photons with helicity $+(-)$. Inset I shows the enlarged spectrum around 1150 eV. (b) MCD spectra around the Eu $M_{4,5}$ region of EuIG at 20 K. The dots are the raw MCD data, while the solid line represents the smoothed MCD data. Inset II shows the enlarged MCD spectrum around 1150 eV.

The absorption spectra were obtained from the total electron yield (TEY) method by measuring the sample current, and the TEY spectra is empirically known to correspond with the x-ray absorption spectra. The incident photon intensity (I_0) was monitored by the mirror current. The photon energy was calibrated by referring to the Ni $L_{2,3}$ edges of NiO and the Ti $L_{2,3}$ edges of TiO_2. The sample current I_1 was normalized by the I_0 monitor current. The XAS intensity I is defined as $I=I_1/I_0$, and the MCD spectrum, as $I_{\mathrm{MCD}}=(I_- - I_+)/\mathrm{MAX}(I_- + I_+)$, where I_+ and I_- denote the absorption intensities with the photon helicity defined as the z axis in Fig. 1. Note that the z axis is opposite to the external magnetic field. A powder sample of EuIG was pasted uniformly on a sample holder using pieces of carbon tape. The temperature of the sample was controlled by a He cryostat. In the measurements at $T=20$ and 300 K, a static magnetic field of 0.4 T was applied to the sample.

B. Experimental Results

Figures 2 and 3 show the results of Eu $3d$ XAS [panels (a)] and MCD [panels (b)) measurements for EuIG at temperatures 20 and 300 K, respectively. The $3d$ XAS in Figs. 2 and 3 consist of the spin-orbit partners M_5 and M_4. In the M_5

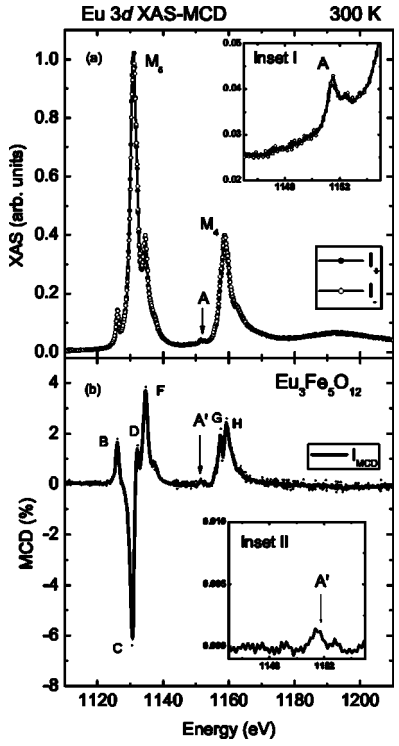

FIG. 3. (a) Experimental Eu 3*d* XAS of EuIG observed at 300 K for circularly polarized photons with helicity + and −. Inset I shows the enlarged spectrum around 1150 eV. (b) MCD spectra around the Eu $M_{4,5}$ region of EuIG at 300 K. Inset II shows the enlarged MCD spectrum around 1150 eV.

region of both figures, three peaks are clearly found, while a peak profile with a shoulder at the high-energy side is found in the M_4 region. Such spectral features are attributed to the multiplet interactions in the 3*d* XAS final state and are a fingerprint of the valency of the Eu element. The observed features are similar to those observed for the Eu^{3+} ion of other Eu compounds[10] and are different from those of the Eu^{2+} ion.[8] Thus, the Eu ions in EuIG are confirmed to be in an almost pure trivalent state at 20 and 300 K. As shown in Figs. 2(a) and 3(a), the overall features of Eu 3*d* XAS at 20 and 300 K are quite similar. However, we find that a structure A appears at the low-energy side of the M_4 edge in the 3*d* XAS at 300 K in Fig. 3(a), which is clearly shown in the enlarged spectra around 1150 eV in inset I of Fig. 3(a). The origin of the temperature change in Eu 3*d* XAS is discussed in Sec. IV A.

As shown in Figs. 2(b) and 3(b), the MCD signals around the $M_{4,5}$ edges are clearly observed at both temperatures 20 and 300 K. The MCD spectra show four peaks around the M_5 edge region, three positive peaks B, D, and F, and a negative peak C, and two positive peaks around the M_4 edge region G and H. As mentioned above, such a complicated feature in the MCD spectra can be attributed to the multiplet interaction in the 3*d* XAS final state. Moreover, we find that the MCD structure A' appears at 300 K (see also the enlarged spectrum in inset II), which is related to the structure A in the Eu 3*d* XAS shown in the upper panel. Though the MCD structures observed at 20 and 300 K are quite similar, except structure A' at 300 K, the intensity of the signal greatly depends on the temperature, i.e., the intensity of peak C, for example, changes from 10% at 20 K to 6% at 300 K.

III. THEORETICAL MODEL

The MCD signals around the $M_{4,5}$ edges of the Eu^{3+} ions are theoretically analyzed by means of an atomic-model calculation including a magnetic-field effect. The Hamiltonian for Eu^{3+} is given by

$$H = H_{\mathrm{SO}} + H_{\mathrm{Coulomb}} + H_{\mathrm{IF}}, \tag{1}$$

where H_{SO} contains the spin-orbit coupling of the $4f$ and $3d$ states and H_{Coulomb}, the multipole part of the $4f-4f$ interaction and $3d-4f$ interaction. The term H_{IF} describes the interaction of the $4f$ states with the internal-magnetic field. For this study, we assume a uniaxial-type field H_{int} along with the z axis (see Fig. 1) at the Eu sites, and thus H_{IF} is given by

$$H_{\mathrm{IF}} = -\mu_z H_{\mathrm{int}} = \mu_B (L_z + gS_z) H_{\mathrm{int}}, \tag{2}$$

where L_z and S_z are the z component of the orbital and spin moments of the Eu $4f$ shell, μ_B is the Bohr magneton, and $\mu_z[=-\mu_B(L_z+gS_z)]$ is the $4f$ magnetic moment of a Eu ion. The g factor in Eq. (2) is assumed to be 2 in the calculation. In the present study, the spin-orbit coupling constants ζ_{nl} in H_{SO} and the Slater integrals F^k and G^k in H_{Coulomb} are numerically estimated within the Hatree-Fock-Slater (HFS) scheme using a Cowan's computation program.[11] The HFS values are as follows: $\zeta_{4f}=0.175(0.202)$ eV for the initial (final) state of 3*d* XAS; $\zeta_{3d}=11.405$ eV; F^k of the $4f-4f$ interaction for the initial (final) state are $F^2=14.083(14.800)$ eV, $F^4=8.839(9.303)$ eV, and $F^6=6.360(6.698)$ eV; F^k and G^k of the $3d-4f$ interaction are $F^2=9.368$ eV, $F^4=4.354$ eV, $G^1=6.657$ eV, $G^3=3.901$ eV, and $G^5=2.695$ eV. However, the 80% values of F^k and G^k are used in the present calculation, which is empirically known as a good prescription for the 3*d* XAS calculation of $4f$ elements.[12] Moreover, ζ_{4f} is reduced to 84.4% of the HFS value in order to reproduce the first excited energy of 0.041 eV of a free Eu^{3+} ion.[4] Such a reduction of ζ_{4f} does not qualitatively affect the calculation for the low-temperature region, but it becomes important especially in the quantitative estimation of the $4f$ magnetic moment and H_{int} at the Eu sites, since both the temperature and magnetic effects for the initial state greatly depend on the first-excited-state energy.

The 3*d* XAS for the circularly polarized incident photons is calculated by

$$I_q(\omega) = \frac{1}{Z}\sum_{f,i} e^{-E_i/k_B T} \left|\langle f|C_q^1|i\rangle\right|^2 \delta(\omega + E_i - E_f), \tag{3}$$

where i and f are the initial state and the final state, respectively; ω, E_i, and E_f are the photon energy, initial-state energy, and final-state energy, respectively; Z is the canonical distribution function for the initial state at the temperature T and is given by $Z=\Sigma_i e^{-E_i/k_B T}$; C_q^1 is the spherical tensor describing the dipole excitation by the circularly polarized photons with helicity $q(=\pm)$. In the present study, it is sufficient to consider the initial state population only for the ${}^7F_J$ terms ($J=0, 1, 2, \ldots,$) of the Eu^{3+} $4f^6$-configuration in order to obtain the convergency.

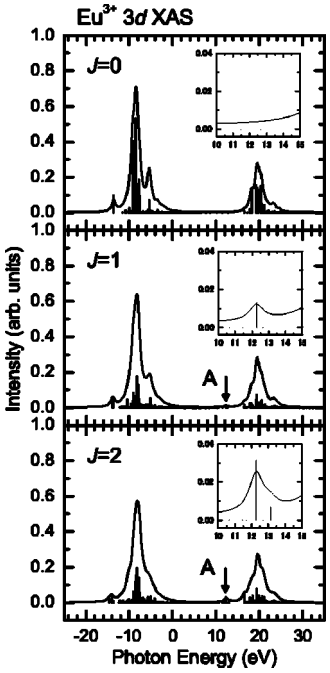

FIG. 4. Theoretical Eu 3*d* XAS for the initial states $^7F_0$ (top panel), $^7F_1$ (middle), and $^7F_2$ (bottom). The inset in each panel shows the enlarged spectrum around the relative photon energy 12 eV.

The initial states with a $4f^6$ configuration and the final states with a $3d^94f^7$ configuration are obtained by numerically diagonalizing the Hamiltonian in Eq. (1). In order to include both the lifetime of the final state and the experimental resolution into the spectral calculation, we take into account the broadening effect for 3*d* XAS by convoluting the spectral function in Eq. (3) with a Lorentz function with the half-width of 0.5 eV at the half-maximum. The MCD signal I_{MCD} is then calculated as

$$I_{\mathrm{MCD}}(\omega) = \frac{I_-(\omega) - I_+(\omega)}{\max[I_-(\omega) + I_+(\omega)]}. \tag{4}$$

IV. THEORETICAL RESULTS AND DISCUSSION

A. Temperature dependence of Eu 3*d* XAS

As shown in Figs. 2(a) and 3(a), Eu 3*d* XAS clearly shows temperature changes. Especially, structure A appears around the photon energy 1152 eV in the 3*d* XAS at 300 K. Such a change can be attributed to the initial state population, since the first ($^7F_1$) and second ($^7F_2$) excited states nearly degenerate with the ground state ($^7F_0$) of the Eu^{3+} ion. According to Wolf and van Vleck,[4] the energy difference between the $^7F_0$ and $^7F_1$ term is 0.041 eV, which corresponds to the temperature 480 K. Thus, in the initial state of 3*d* XAS, the thermal population of the excited states $^7F_1$ and $^7F_2$ cannot be ignored in the vicinity of 300 K.

In order to see the contributions from the ^7F_J terms, we show in Fig. 4 the calculated 3*d* XAS for the initial states $^7F_0$ (top panel), $^7F_1$ (middle), and $^7F_2$ (bottom), where the insets show the enlargement of each spectrum around the relative photon energy of 12 eV. In this figure, the spectra are calculated for unpolarized light and by omitting the H_{IF} term in Eq. (2) in order to show the *pure* temperature effect. It is found that the M_5 structure differs among the spectra for $J=0$, 1, and 2, i.e., the intensities of side peaks around the main peak become weaker going from $J=0$ to 2. Moreover, it is found that a structure A appears around the relative photon energy of 12 eV in the spectra for $J=1$ and 2 (see also the insets).

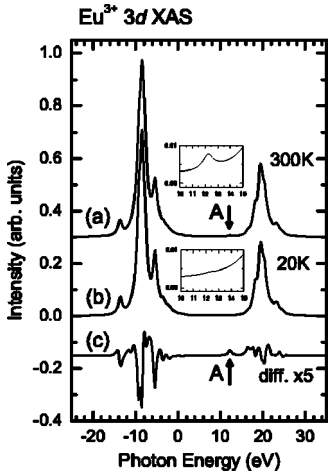

FIG. 5. Temperature dependence of Eu 3*d* XAS. The theoretical 3*d* XAS calculated for $T=20$ K (a) and 300 K (b) are shown. The curve (c) is the difference of spectra between (a) and (b).

Figures 5(a) and 5(b) show the theoretical 3*d* XAS at 20 and 300 K, respectively, where the spectra are calculated for unpolarized light and with the internal field effect due to H_{IF}. We see that the characteristic features observed in the experiment in Figs. 2 and 3 are reproduced by the theoretical spectra in Figs. 5(a) and 5(b), i.e., the intensities of the side peaks around the M_5 structure become weaker, and the structure A around the relative photon energy of 12 eV appears in the spectra for 300 K. The temperature dependence of the 3*d* XAS is more clearly shown in the difference spectra in Fig. 5(c). Such changes in the spectra are interpreted as the contributions from the thermally populated initial states with $J=1$ and 2, as shown in Fig. 4. Actually, the thermal population of J multiplets is given as follows: 100%($^7F_0$) for 20 K and 74%($^7F_0$), 25%($^7F_1$), and 1%($^7F_2$) for 300 K. (It should be noticed that the use of term ^7F_J is for convention, since they are quantum-mechanically mixed with each other through H_{IF}.)

B. Origin of the MCD signal of Eu^{3+} around the Eu $M_{4,5}$ edges

In the ground state, an isolated Eu^{3+} ion dose not have a finite $4f$ magnetic moment since the Hund's rule predicts the $^7F_0$ state as the ground state for the $4f^6$ configuration. Consequently, the MCD signal cannot be expected for a low-temperature measurement if Eu^{3+} ions are regarded as isolated ones in materials. Therefore, in order to explain the MCD signal observed at 20 K in Fig. 2, we must take into

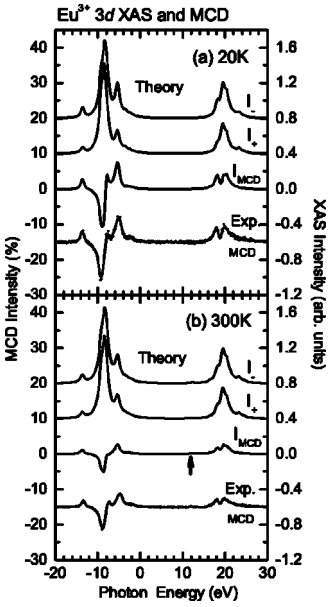

FIG. 6. Comparison between theoretical MCD spectra (solid line) and experimental spectra (dots with solid line) for 20 K (a) and 300 K (b). The theoretical 3*d* XAS $I_{\pm}$ is also shown in both panels for the incident photon helicity + and −.

account the internal field in EuIG. In fact, in the initial state of Eu 3*d* XAS, the $^7F_0$ state is expected to quantum-mechanically hybridize with higher multiplets as $^7F_1$ and $^7F_2$ through the interaction H_{IF} in Eq. (2), which can cause the nonzero MCD signal in the low-temperature measurement.

Figure 6 shows a comparison between the experimental and theoretical MCD spectra at 20 K [panel (a)] and 300 K [panel (b)], where the theoretical MCD spectra are shown by solid lines and the experimental MCD spectra are shown by dots with solid lines at the bottom of each panel. In addition, the theoretical 3*d* XAS are shown by solid lines denoted with I_- and I_+ in both panels. In the calculation of the spectra in Fig. 6, we assume the internal field in Eq. (2) to be 70 (55) T for 20 (300) K so as to reproduce the experimental spectra. As a consequence, the nonzero MCD signal appears in the spectrum at 20 K, as expected, and the spectral features observed in the MCD measurement is almost reproduced by the theoretical spectrum. As the temperature is raised to 300 K, the theoretical MCD signal becomes weaker around the whole photon energy region, and a structure indicated by an up-arrow appears in the MCD spectra. The former is attributed to the fact that the internal field at 300 K becomes weaker due to the thermal averaging effect, while the latter comes from structure A shown in the excited-state absorption in Fig. 4. As shown here, the most features observed in the experiment are reproduced by the theoretical calculation.

C. Magnet-optical sum rule for Eu^{3+}

According to the so-called L_z sum rule, one of the well-known sum rules in the XAS-MCD study, the $4f$ orbital magnetic moment can be related with the difference between the spectral functions $I_- - I_+$. More precisely, the expectation value $\langle L_z \rangle$ for the $4f$ shell is given by the formula[6,7]

$$\frac{\int_{M_4+M_5}(I_- - I_+)d\omega}{\int_{M_4+M_5}(I_- + I_+ + I_0)d\omega} = \frac{\langle L_z \rangle}{3(14 - n_f)}, \tag{5}$$

where $I_q(q=0,\pm)$ represents the spectral function of the $3d \rightarrow 4f$ absorption process for the incident-photon helicity q and n_f is the $4f$ electron number of the R ion in the ground state. The integrals in the left-hand side of Eq. (5) are taken over the whole energy region around the M_4 and M_5 edges. The L_z sum rule generally holds for x-ray absorption regions related with the dipole excitation, such as the M_5+M_4 region of rare-earth compounds and the L_3+L_2 region of transition-metal compounds, under a plausible assumption that the radial part of the valence-electron wave function does not depend on the energy around the edges.

In the case of the Eu^{3+} ion in the internal field, the induced $4f$ magnetic moment in the ground state $|g\rangle$ can be directly linked with the L_z sum rule as follows: the ground-state average of the z component of the $4f$ magnetic moment $\mu_z = -\mu_B(L_z + 2S_z)$ is generally given by

$$\langle g|\mu_z|g\rangle = -2\mu_B\langle g|J_z|g\rangle + \mu_B\langle g|L_z|g\rangle. \tag{6}$$

However, since the J_z remains as a good quantum number even if there is a uniaxial perturbation as in Eq. (2), $\langle g|J_z|g\rangle$ for Eu^{3+} is kept to be 0 as long as the internal-field H_{int} is not so strong, and, thus, the order of the lowest few energy levels is not reversed. Thus, we obtain the formula

$$\langle g|\mu_z|g\rangle = \mu_B\langle g|L_z|g\rangle, \tag{7}$$

for Eu^{3+} at $T=0$ K, and we can estimate the $4f$ magnetic moment by directly accessing the L_z sum rule given in Eq. (5).

At a finite temperature, however, we must also consider the contribution from the J_z term, since the thermal population in the lowest few excited states with nonzero M_J value, such as $^7F_{1,M_J=\pm 1}$, cannot be negligibly small in the vicinity of 300 K. In fact, considering the thermal population in the $^7F_1$ states with $M_J=0$ and ±1, the *linear response* of the thermal average $\langle J_z \rangle$ at the temperature T is given by

$$\langle J_z \rangle_{\mathrm{linear}} = -\frac{3\mu_B}{k_B T}\frac{e^{-\Delta_{10}/k_B T}}{1 + 3e^{-\Delta_{10}/k_B T}}, \tag{8}$$

as derived in the Appendix , where Δ_{10} denotes the energy difference $E_1 - E_0$ between the $J=0$ and $J=1$ states of Eu^{3+} free from the magnetic interaction in Eq. (2), i.e., unperturbed Eu^{3+}. Then, the ground-state relation in Eq. (7) no longer exactly holds at finite temperature.

Figure 7 illustrates the relation between $\langle \mu_z \rangle$ (solid-line curve) and $\mu_B\langle L_z \rangle$ (dashed-line curve) as a function of the temperature T, where the internal field is fixed as $H_{\mathrm{int}} = 70$ T. The curves are obtained from the atomic model calculation considering the thermal population in the *perturbed* ^7F_J states from $J=0$ to 5. We find that, as expected from Eq. (8), the $\langle J_z \rangle$ value gradually changes from 0 to a negative one when the temperature is raised from 0 K. This change comes mainly from the unbalance in the thermal populations for the

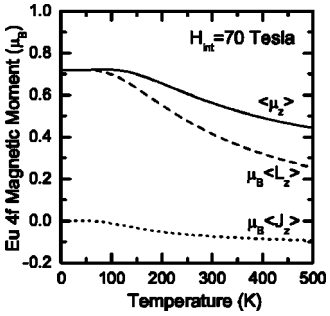

FIG. 7. Theoretical $\langle\mu_z\rangle$, $\mu_B\langle L_z\rangle$, and $\mu_B\langle J_z\rangle$ against the temperature, where $H_{\rm int}$ is fixed to be 70 T. In the low-temperature region ($T\leqslant 50$ K), $\langle\mu_z\rangle$ coincides with $\mu_B\langle L_z\rangle$, while, in the higher-temperature region, they are separated from each other because of the thermal contributions from such a state with $M_J\neq 0$.

$^7F_{1,M_J=-1}$ and $^7F_{1,M_J=+1}$ states, i.e., the former has more weight than the latter when the internal field is applied, since the energy of the former becomes lower than that of the latter due to the Zeeman effect for the $J=1$ states. Consequently, when the temperature is raised from 0 K, the thermal average $\langle\mu_z\rangle$ becomes to deviate from $\mu_B\langle L_z\rangle$ following the relation $\langle\mu_z\rangle=-2\mu_B\langle J_z\rangle+\mu_B\langle L_z\rangle$, among the thermal average quantities. The overall behavior of $\langle\mu_z\rangle$ against the temperature shows the typical behavior of the van Vleck-type magnetism, i.e., a plateau in the low-temperature region and a gradual reduction at the high-temperature region, which can be well simulated as the *linear response* for the internal field

$$\langle\mu_z\rangle_{\rm linear}=\frac{8\mu_B^2H_{\rm int}}{\Delta_{10}}g(T), \tag{9}$$

where $g(T)$ describes the temperature dependence and is given by

$$g(T)=\left[1+\left(\frac{9\Delta_{10}}{16k_BT}+\frac{15\Delta_{10}}{8\Delta_{21}}-1\right)e^{-\Delta_{10}/k_BT}\right]\times(1+3e^{-\Delta_{10}/k_BT})^{-1}. \tag{10}$$

In the derivation of Eq. (10), which is given in the Appendix, thermal populations for only the $^7F_0$ and $^7F_1$ states are considered. Note that $g(0)=1$ and, thus, the coefficients for $g(T)$ in Eq. (9) give a linear response at 0 K.

Using the L_z sum rule in Eq. (5) and the expression in Eq. (7), we can estimate the $4f$ magnetic moment at low temperature directly from the MCD measurements. In the present study, the value of 0.73 μ_B per a Eu^{3+} ion was obtained at 20 K. Actually, we have replaced I_0 in Eq. (5) by $(I_-+I_+)/2$ in this estimation, which would induce a negligibly small error. Note that the magnetic-moment value obtained in the present study is consistent with that obtained from magnetization measurements.[4]

Here, we should emphasize the advantage of the MCD study of Eu^{3+} ion in EuIG. In conventional magnetization measurements, a precise estimation of the magnetic moments of Eu^{3+} is difficult, since such measurements would yield the overall magnetic response from both Fe and Eu moments and the magnetic moment of Eu ions is much smaller than that of Fe ions. However, in the MCD measurements, the magnetic property of Eu can be directly accessed and precisely estimated owing to the advantage of the element and orbital selectivity of this technique. However, in order to precisely estimate the $4f$ magnetic moment at finite temperature from the XAS-MCD study, further analysis is required, since a simple relation such as that given in Eq. (7) no longer holds exactly in the high-temperature region, as described above.

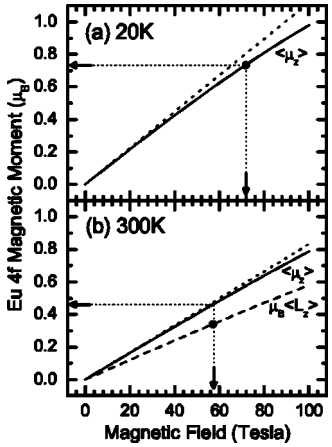

FIG. 8. Theoretically obtained $4f$ magnetic moment $\langle\mu_z\rangle$ (solid line curves) and $4f$ orbital magnetic moment $\mu_B\langle L_z\rangle$ (dashed line curves) of a Eu ion against the internal field. In panel (a) for $T=20$ K, both curves almost completely coincide with each other, while, in panel (b) for $T=300$ K, they are separated due to the thermal population in such a state with $M_J\neq 0$. $\langle\mu_z\rangle$ is well simulated by dotted lines obtained from Eqs. (9) and (10). The black dot in each panel shows the experimental value of $\mu_B\langle Lz\rangle$, obtained from the L_z sum rule for XAS-MCD measurements.

D. $4f$ magnetic moment and internal field

As discussed so far, the internal field induces the finite $4f$ magnetic moment of the Eu^{3+} ion, which is approximately described as the linear response in Eq. (9), and thus causes the MCD in the Eu $3d$ XAS. Therefore, in addition to the $4f$ magnetic moment, the internal field at the Eu sites can be estimated from the MCD measurements.

Figure 8 shows the $H_{\rm int}$ dependence of the thermal averages $\langle\mu_z\rangle$ (solid-line curves) and $\mu_B\langle L_z\rangle$ (dashed-line curves), where the temperature is fixed to be 20 and 300 K in panels (a) and (b), respectively. The curves in Fig. 7 are theoretically obtained using the present model system. We see that both $\langle\mu_z\rangle$ and $\mu_B\langle L_z\rangle$ monotonously increase when the internal field becomes stronger. Such a behavior of the $\langle\mu_z\rangle$ curves can be well simulated by the linear response $\langle\mu_z\rangle_{\rm linear}$ (dotted curves) in Eq. (9). It should be noted that the two curves in panel (a) almost completely coincide with each other, since the deviation from Eq. (7) remains negligibly small at the low temperature of 20 K. This situation is in contrast with the $\langle\mu_z\rangle-\mu_B\langle L_z\rangle$ relation at 300 K in panel (b), where the thermal population in the lowest few excited states with a nonzero M_J value cannot be ignored and contributes to the deviation.

Using the curves shown in Fig. 8, we can estimate both the $4f$ magnetic moment of the Eu ion and the internal magnetic field at the Eu sites from MCD measurements. The closed circles in Figs. 8(a) and 8(b) show the $\mu_B\langle L_z\rangle$ value experimentally obtained from the MCD spectra in Figs. 2 and 3 using the L_z sum rule in Eq. (5). Then, the internal field at the Eu sites of EuIG is estimated to be 72 ± 7 T at 20 K and 57 ± 3 T at 300 K, while the $4f$-magnetic moment of Eu ions is estimated to be 0.73 μ_B at 20 K and 0.46 μ_B at 300 K. The value of the internal field at 20 K is consistent with that obtained from the Mössbauer measurements by Nowik and Ofer,[5] but the value at 300 K is considerably larger than the 33.5 ± 5 T obtained by them. This discrepancy at 300 K can be responsible for the inadequate statistics and the low-energy resolution in the Mössbauer measurements, as they commented in Ref. 8.

As demonstrated so far, both the statistical accuracy and energy resolution in the XAS-MCD measurement are high enough to estimate the internal magnetic field at the Eu site with accuracy. Moreover, the MCD technique can easily investigate the temperature dependence. Thus, we propose that the MCD measurement can be a good probe for the local internal-magnetic field in ferromagnetic materials including Eu^{3+} or Sm^{2+} which also has the $4f^6$ configuration.

V. CONCLUSION

The electronic structure of EuIG is investigated by means of x-ray absorption spectroscopy (XAS) and magnetic circular dichroism (MCD) measurement. This study succeeds in the observation of the MCD around the Eu $M_{4,5}$ edges, which is caused by the finite $4f$ magnetic moment of Eu^{3+} induced by the van Vleck-type magnetism through the internal magnetic field of EuIG. The Eu $3d$ XAS and the MCD spectra observed at the temperatures 20 and 300 K clearly show the temperature change: The MCD signal intensity significantly changes between 20 and 300 K and a spectral structure appears at the low-energy side of the Eu M_4 edge in both the $3d$ XAS and MCD spectra at 300 K.

The observed spectra are analyzed by means of the full-multiplet atomic-model calculation for Eu^{3+}, including the internal-field effect. The experimentally observed features in the $3d$ XAS and MCD spectra are almost reproduced by theoretical calculations. Because of quantum mechanical mixing among ^7F_J terms with $J=0$, 1, and 2 through the internal field, the Eu^{3+} ion has a nonzero magnetic moment even in its ground state. This is the origin of the MCD signal observed at 20 K. Moreover, the structure observed at 300 K is attributed to the contributions from the $J=1$ and 2 states, which are thermally populated in the initial state of the system. The magnet-optical sum rule for Eu^{3+} is discussed, and it is shown that both the $4f$ magnetic moment and internal field can be estimated using the so-called $\langle L_z\rangle$ sum rule. From a comparison between the experiment and the theory, the net magnetic moment of the Eu^{3+} ion, which is induced by the van Vleck-type magnetism thorough the internal magnetic field of EuIG, is estimated to be 0.73 μ_B at 20 K and 0.46 μ_B at 300 K, and the internal-magnetic field at the Eu sites is estimated to be about 72 T at 20 K and 57 T at 300 K. We developed the linear response model to treat perturbative induced magnetic moments and showed the $4f$ magnetic moment of the Eu^{3+} ion as the application of this model. Finally, we studied the characteristic contribution from thermal and the magnetic excitation to the excited states saparetely and conclude that the thermal excited states of Eu^{3+} ions are the linear combination between $J=0$, 1, and 2 and that the magnetic-field-excited state is the quantum-mechanically mixed state of the ground and excited states.

APPENDIX: LINEAR RESPONSE

The linear responses of J_z and μ_z in Eqs. (8) and (9) for the internal magnetic field $H_{\rm int}$ are derived from a standard formula of the linear response theory[13]

$$\langle A\rangle = \langle A\rangle_0 - \int_0^\beta d\tau\langle V(\tau)A\rangle_0. \tag{A1}$$

In this equation, $\langle A\rangle$ and $\langle A\rangle_0$ are the thermodinamical average of an operator A in the perturbed and unperturbed systems, respectively, $\beta=1/k_BT$, and $V(\tau)=e^{\tau H_0}Ve^{-\tau H_0}$, where H_0 is the unperturbed Hamiltonian and V is the perturbation.

In the case of Eu^{3+}, the first term in Eq. (A1) vanishes for both J_z and μ_z because of the spherical symmetry in the unperturbed system. However, if the perturbation, $V=-\mu_zH_{\rm int}$ in the present case, is switched on, we obtain a finite response through the formulas

$$\langle J_z\rangle = H_{\rm int}\int_0^\beta d\tau\langle\mu_z(\tau)J_z\rangle_0, \tag{A2}$$

and

$$\langle \mu_z\rangle = H_{\rm int}\int_0^\beta d\tau\langle\mu_z(\tau)\mu_z\rangle_0. \tag{A3}$$

The right-hand sides of Eqs. (A2) and (A3) can be estimated within the *LS*-coupling scheme for the unperturbed system. In the present study, it is sufficient to consider thermal populations only in the lowest few levels, i.e., ^7F_J states with $J=0$ or 1 of Eu^{3+}. Then, Eq. (A2) is approximated as

$$\langle J_z\rangle = H_{\rm int}\int_0^\beta d\tau\sum_{J=0}^{1}\sum_{M_J=-J}^{J} e^{-\beta E_J}M_J\langle JM_J|\mu_z|JM_J\rangle, \tag{A4}$$

which can be further reduced using the Wigner-Eckart theory with the reduced matrix element for the ^7F_J terms as

$$\begin{aligned}\langle J\|\mu\|J'\rangle = &-2\mu_B\delta_{JJ'}\sqrt{(2J+1)(J+1)J}\\ &+(-1)^{J'+1}2\sqrt{21}\mu_B\sqrt{(2J+1)(2J'+1)}\\ &\times\begin{Bmatrix}3 & 3 & 1\\ J & J' & 3\end{Bmatrix}.\end{aligned} \tag{A5}$$

Using a standard table for $3j$ and $6j$ symbols, we obtain Eq. (8).[14] Similarly, Eq. (A3) can be approximated as

$$\langle J_z \rangle = H_{\mathrm{int}} \int_0^\beta d\tau \sum_{J=0}^{1} \sum_{J'=0}^{2} \sum_{M_J, M_J'} e^{-\beta E_J} e^{\tau (E_J - E_{J'})} \times |\langle J M_J | \mu_z | J' M_J' \rangle|^2, \quad \text{(A6)}$$

considering the thermal population only for the $J=0$ and $J=1$ states, which can be reduced to Eq. (9) using the Wigner-Eckart theory and Eq. (A5).

ACKNOWLEDGMENTS

The authors gratefully thank the JASRI staff, especially, Dr. H. Tanaka, Dr. M. Takao, and Dr. T. Matsushita, for their help in helicity switching of the undulator in the experiment. The authors would also like to thank the JAERI soft x-ray staff, especially, Dr. A. Yoshigoe and Dr. T. Nakatani, for supporting the beam-line BL23SU in SPring-8.

[1] S. Geller and M. A. Gilleo, J. Phys. Chem. Solids **3**, 30 (1957).
[2] E. P. Wolfarth, *Ferro Magnetic Materials*, Vol. 2 (Elsevier Science Publishers, Amsterdam, 1980), p. 1–54.
[3] L. Nèel, Ann. Phys. **3**, 137 (1948).
[4] W. P. Wolf and J. H. van Vleck, Phys. Rev. **118**, 1490 (1960).
[5] I. Nowik and S. Ofer, Phys. Rev. **132**, 241 (1963).
[6] P. Carra, B. T. Thole, M. Altarelli, and X. Wang, Phys. Rev. Lett. **70**, 694 (1993).
[7] B. T. Thole, P. Carra, F. Sette, and G. van der Laan, Phys. Rev. Lett. **68**, 1943 (1992).
[8] B. T. Thole, G. van der Laan, J. C. Fuggle, G. A. Sawatzky, R. C. Karnatak, and J. M. Esteva, Phys. Rev. B **32**, 5107 (1985).
[9] A. Agui, A. Yoshigoe, T. Nakatani, T. Matsushita, Y. Saitoh, A. Yokoya, H. Tanaka, Y. Miyahara, T. Shimada, M. Takeuchi, T. Bizen, S. Sasaki, M. Takao, H. Aoyagi, T. P. Kudo, K. Satoh, S. Wu, Y. Hiramatsu, and H. Ohkuma, Rev. Sci. Instrum. **72**, 3191 (2001).
[10] M. Mizumaki, Y. Saitoh, A. Agui, K. Yoshii, A. Fujimori, and S. Nakamura, J. Synchrotron Radiat. **8**, 440 (2001).
[11] R. D. Cowan, *The Theory of Atomic Structure and Spectra* (University of California Press, Berkeley, CA, 1981).
[12] H. Ogasawara, A. Kotani, K. Okada, and B. T. Thole, Phys. Rev. B **43**, 854 (1991).
[13] See for example, G. D. Mahan, *Many-Particle Physics*, 3rd Ed. (Kluwer Academic/Plenum Publishers, New York, 2000).
[14] See for example, I. Lindgren and J. Morisson, *Atomic Many-Body Theory* (Springer-Verlag, Berlin, 1985).